Preprints (www.preprints.org) | NOT PEER-REVIEWED | Posted: 28 December 2022 doi:10.20944/preprints202212.0528.v1

Disclaimer/Publisher's Note: The statements, opinions, and data contained in all publications are solely those of the individual author(s) and contributor(s) and not of MDPI and/or the editor(s). MDPI and/or the editor(s) disclaim responsibility for any injury to people or property resulting from any ideas, methods, instructions, or products referred to in the content.

Article

High Resolution Magnetoelectric Sensor and Low-frequency Measurement using Frequency up-conversion Technique

Kunyu Sun,[1] Zhihao Jiang,[1] Chengmeng Wang,[1] Dongxuan Han,[2] Zhao Yao,[2] Weihua Zong,[2] Zhejun Jin,[2] and Shandong Li[1,2,*]

[1]College of Physics, Center for Marine Observation and Communication, Qingdao University, Qingdao 266071, China
[2]College of Electronics and Information, Qingdao University, Qingdao266071, China
*Correspondence: lishd@qdu.edu.cn

Abstract: Magnetoelectric (ME) sensor is a new type magnetic sensor with ultrahigh sensitivity, low power consumption, and suitable for the measurement of low frequency weak magnetic field. In this study, metglas/PZT-5B ME sensor with a mechanical resonance frequency f_{res} of 60.041 kHz was prepared. It is interesting to note that its magnetic field resolution reaches 0.20 nT at f_{res} and 0.34 nT for DC field, respectively. In order to measure the ultralow frequency AC magnetic fields, a frequency upconversion technique was employed. Under this technique, a limit of detection (LOD) of AC magnetic field lower than 1 nT at 8 Hz is obtained, and the minimum LOD of 0.51 nT is achieved at 20 Hz. The high resolution ME sensor with sub-pT level is promising in the field of low frequency weak magnetic field measurement technology.

Keywords: magnetoelectric sensors; frequency upconversion technique; piezomagnetic material; low-frequency weak magnetic field

1. Introduction

With the development of the information age, the internet of things in the world requires all kinds of sensors to accurately detect the physical properties of different substances, leading to a widely application of sensors. For example, microelectro mechanical systems (MEMS) sensors can work in a variety of environments [1-6]. The magnetic sensor is one kind of the most important sensors. According to the working principle, magnetic sensors can be divided into the following types: magnetoresistance-type (for example, anisotropic magnetoresistance, giant magnetoresistance, tunneling magnetoresistance), magnetic-flux-type (flux-gate magnetometer, optic-pumping atomic magnetometer, proton precession magnetometer, and superconducting quantum interference devices), magnetic-field-type (giant magnetoimpedance, magnetoelelctric coupling sensor), and so on. The magnetoresistance-type sensors have relatively lower magnetic field resolution. The magnetic-flux-type sensors exhibit very high magnetic field resolution, but the magnetic field resolution strongly depends on the dimension of the sensors. The reduction of dimension will result in a dramatically deterioration of magnetic field resolution [7-10]. In contrast, the magnetic-field-type sensors are proportional to the field intensity, not as strongly dependent on the sensor dimension as flux-type one [11-13]. Therefore, the ME sensor is very beneficial for the miniaturization and integration. At present, ME sensors have been used for non-contact positioning and navigation, such as geomagnetic field detection and brain magnetic field imaging [14-20].

ME sensors, based on the magnetoelectric coupling effect, can timely transmit the magnetic field signals to a voltage, mediated in the interfacial stress σ [3, 21-24]. A good ME sensor should have a high ME coupling coefficient α_{ME}, thus a large output voltage is available under a certain external magnetic field. The ME conversion efficiency reaches a maximum when the frequency of the external AC field is close to the mechanical resonance frequency f_{res} of the sensor. A DC bias magnetic field H_{bias} usually exerts to the

© 2022 by the author(s). Distributed under a Creative Commons CC BY license.

Preprints (www.preprints.org) | NOT PEER-REVIEWED | Posted: 28 December 2022 doi:10.20944/preprints202212.0528.v1

piezomagnetic layer to maximize the piezomagnetic coefficient d_m. Therefore, the best magnetic field sensitivity of ME sensor with an optimized α_{ME} should be working at f_{res} under an optimal DC bias magnetic field [10, 25-28]. Recently, the research work is focused on reducing f_{res} and improving α_{ME} of the ME sensors. E. Quandt in Kiel University, Germany enhanced the magnetoelectric coupling coefficient up to $|\alpha_{ME}|_{max} = 6.9\ \mathrm{kV/cm \cdot Oe}@H_{bias} = 2.4\ \mathrm{Oe}$ in AlN/FeCoSiB thin film sensor by adjusting the resonance frequency range of Si cantilever beam [29].

In general, the frequency of weak magnetic field to be measured is usually lower than 1 kHz (such as, magnetoencephalography, magnetocardiography, and underwater/underground mineral resources), while the typical operating frequency (f_{res}) of bulk ME sensor is several tens of kHz. Moreover, the magnetic field resolution dramatically reduces with deviation from the f_{res}. In order to sensitively measure ultra-low frequency magnetic field signals by using ME sensor vibrating at resonant frequency f_{res}, a frequency upconversion technique is employed in this study. If a low-frequency (f_{tbm}) magnetic field to be measured is exerted on the ME sensor vibrating at its mechanical resonance f_{res}, two shoulder peaks will appear on both sides of the main peak at the resonance frequency f_{res} after Fourier transform. The frequency shifts from the main peak are $\pm f_{tbm}$, respectively, and the peak height was proportional to the measured magnetic field. After magnetic field calibration, the magnitude of the measured low frequency weak magnetic field signal can be obtained via measuring the height of the shoulder peaks [30-33]. In general, the limit of detection (LOD) depends on the dimension of ME sensor and the operating frequency, and the LOD for the thin-film sensor is better than that of bulk one, and the LOD for AC field is smaller than that for DC one as well. For example, the LOD of AC magnetic field for metal glass/lead niobium magnesium-Lead titanate (Metglas/PMN-PT) sensor, reported by S. Zhang in University of Wollongong, is 2 pT, while that of DC magnetic field is only 200 pT [34]. Z. Chu in Peking University also reported a LOD of 115 pT in a Metglas/PMN-PT sensor at 10 Hz [35].

As for the thin-film ME sensors, they are promising because of their lower operating frequency and magnetic field sensitivity. E. Quandt in Kiel University widely studied the film ME sensors composed of soft magnetic films and AlN ferroelectric layer. He reported that the magnetoelectric properties of AlN/FeCoSiB can be regulated by adjusting NiTi substrate, a very low frequency of 273 Hz and a LOD of 110 $\mathrm{pT}/\sqrt{\mathrm{Hz}}$ were obtained. In addition, an ultrahigh sensitivity of 64 kV/T under a zero bias magnetic field was obtained through the converse ME modulation of thin-film Si cantilever composites, the LOD of 210 $\mathrm{pT}/\sqrt{\mathrm{Hz}}$ at 1 Hz and 70 $\mathrm{pT}/\sqrt{\mathrm{Hz}}$ at 10 Hz were achieved. Even for similar systems, a linear resolution of 1.2 nT at 200 mHz can be obtained by combining mesoscale thin film cantilever beams with pickup coil readout [18,27,36,37]. However, thin-film ME sensors require complex micromachining techniques and have a high cost. The preparation of bulk ME sensor is simple, the technology is flexible, and it has a good development prospect. Therefore, this study focuses on exploring the bulk ME sensor and its measurement method.

2. Experimental

A FeCoSiB metglas sheet with dimension of $22^{\mathrm{length}} \times 2^{\mathrm{width}} \times 0.03^{\mathrm{thickness}}\ \mathrm{mm}^3$ was bonded to a lead zirconate titanate Pb(Zr,Ti)O_3-5B (PZT-5B) sheet with dimension of $25 \times 2 \times 0.5\ \mathrm{mm}^3$ using AB epoxy adhesive produced by 3M company. The PZT-5B sheet is 3 mm longer than Metglas sheet because the reserved part of PZT-5B was used to stick the enameled wire to measure the output ME voltage. The upper and lower sides of PZT are coated with silver glue in advance, and then the piezoelectric PZT-5B was polarized in the thickness direction under a voltage of 3.0 kV.

The performance of the ME sensor were carried out by a home-made ME test system, as shown in Figure 1. The prepared ME sensor is put in a long-straight solenoid magnetic field generator. An AC voltage signal provided by a lock-in amplifier (Stanford, model

Preprints (www.preprints.org) | NOT PEER-REVIEWED | Posted: 28 December 2022 doi:10.20944/preprints202212.0528.v1

SR830) was amplified by a power amplifier, then input into the above long-straight solenoid to generate AC magnetic field H_{ac}. The long-straight solenoid is placed along the axis center of the Helmholtz coils. The DC bias magnetic field H_{bias} was generated by the Helmholtz coils supplied by a DC power supply (YL2420). The variation of H_{ac} (also called the magnetic field to be measured H_{tbm}) will cause a strain in the piezomagnetic metglas (FeCoSiB amorphous ribbon in this study) due to the magnetostrictive effect. This strain will exert on the piezoelectric PZT-5B through the AB epoxy adhesive, leading to a voltage via the piezoelectric effect, mediated by the interface stress. The output voltage of ME sensor is amplified by the lock-in amplifier, then transmitted and processed by a home-made Labview program. This measurement instrument is used to explore some performances of ME sensors, for example, to find out the optimal working point, including the mechanical resonance frequency f_{res} and DC bias field H_{bias}, and to measure the LOD, magnetic field resolution and sensitivity of ME sensors. In addition, the magnetic field resolution of DC and AC field at f_{res} or ultra-low frequencies of ME sensors can be measured by improving the instrument. Under a certain DC field (around the optimal DC bias field), the output voltage V_{out} versus frequency (V_{out}-f) curve can be obtained by scanning the frequency from 0 to 100 kHz. The frequency at the peak of V_{out}-f curve is the mechanical resonance frequency f_{res}. After that, setting the lock-in amplifier at f_{res} and scanning the DC field H, the V_{out}-H curve can be obtained. The magnetic field at the maximum V_{out} is the optimal magnetic field the optimal H_{bias}.

2.1. AC field resolution at f_{res}

Set the frequency of lock-in amplifier at f_{res}. The AC magnetic field strength H_{ac}, exerted on the ME sensor, can be tuned by the output voltage of the lock-in amplifier. For a fixed H_{ac}, a stable ME output voltage V_{out} can be obtained from the lock-in amplifier. Thus, a V_{out} platform will be appeared in V_{out}–time curve. Since V_{out} is proportional to H_{ac}, decreasing H gives rise to a series of steps in the V_{out}–time curve. The AC field resolution limit can be approaching by decreasing H_{ac} till the steps are indistinguishable.

2.2. DC field resolution

To test the DC field resolution, the ME sensor is put into the center of an additional small solenoid, and then they are put into the center of the long-straight solenoid. The DC magnetic field, as a field to be measured H_{tbm}^{DC}, is generated by this small solenoid, supplied by Keithley 2400 source meter, while the driving AC magnetic field with frequency of f_{res} is still provided by the long-straight solenoid, supplied by lock-in amplifier. The optimal DC bias field H_{bias} is also generated by Helmholtz coils. Therefore, at this moment, the ME sensor is working at f_{res} and at field of H_{bias}+H_{tbm}^{DC}. Since the H_{tbm}^{DC} is much smaller than H_{bias}, the ME sensor actually operates in the perturbation state of the optimal DC bias field. Reduce the H_{tbm}^{DC} till the V_{out}-time step becomes indistinguishable, and the minimum value of H_{tbm}^{DC} (i.e. the DC field resolution) can be found out.

2.3. AC field resolution at ultralow frequency

During the measurement of AC field resolution at ultralow frequency, the AC magnetic field power supply of lock-in amplifier is replaced by a signal generator (RIGOL DG2102) because the signal generator is easier to adjust the signal modulation frequency and depth. However, the V_{out} of the ME sensor is still received and processed by SR830 lock-in amplifier. Although a high AC magnetic field resolution can be achieved at f_{res}, it will dramatically reduce when the operating frequency is deviated from f_{res}. This can be attributed to the rapid reduction of ME coupling efficiency. This characteristic of ME sensor shows that it is not suitable for the direct measurement of ultra-low frequency magnetic field. Therefore, it is necessary to find out a way to measure the ultralow frequency magnetic field by taking advantage of the extremely high sensitivity of the ME sensors. In this study, a frequency up-conversion technique (FUCT) was proposed for measuring the

Preprints (www.preprints.org) | NOT PEER-REVIEWED | Posted: 28 December 2022 doi:10.20944/preprints202212.0528.v1

ultralow frequency magnetic field using ME sensor. The signal generator outputs two signals of different frequencies, one with the frequency of f_{res} as the reference signal, and the other as the signal to be measured H_{tbm}^{AC} with very low frequency (f_{ac}=8 Hz for instance). A mixed signal modulated by the low frequency signal is fed into a long straight solenoid, which in turn applies the resulting magnetic field to the ME sensor. The output voltage from the ME sensor is picked up by an oscilloscope (Tektronix MDO34), instead of a lock-in amplifier. It can be seen that two voltage shoulder peaks will appear in the left (f_{res}-f_{ac}) and right (f_{res}+f_{ac}) around f_{res}, respectively, with a frequency shift Δf of $\pm f_{ac}$ from f_{res}. The voltage amplitude of the shoulder peak is proportional to the strength of the low-frequency modulation field H_{tbm}^{AC}. The AC field resolution H_{rsl}^{AC} can be obtained by reducing the low-frequency H_{tbm}^{AC} till the shoulder peaks are undetectable. Change the modulation frequency, and repeat the above operation, the frequency dependence of H_{rsl}^{AC} can be obtained.

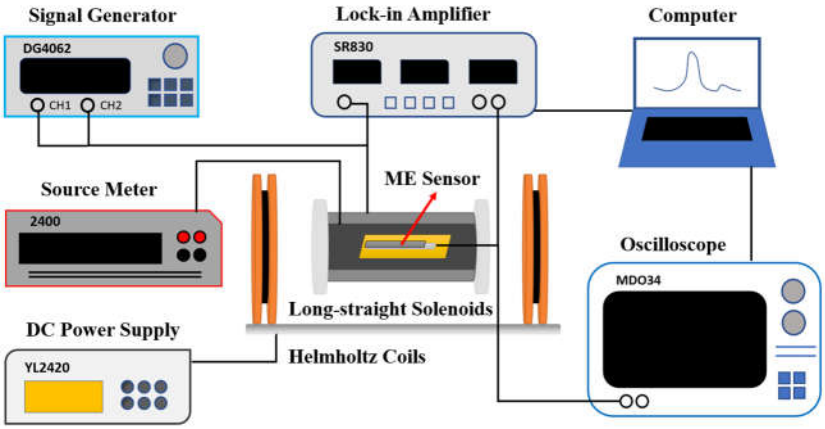

Figure 1. The schematic show of the principle of the ME test system (The actual wiring method can be adjusted according to the test types).

3. Results and discussion

The AC field frequency dependence of V_{out} of the ME sensor was detected by scanning the AC field frequency in the range of 1-70 kHz under zero DC bias field (Figure 2a). The center frequency of 60.041 kHz was observed. However, when the AC field frequency is scanned under a DC bias field of 2.5 Oe, the peak frequency is shifted from 60.041 kHz to 60.101 kHz (Figure 2b). The resonance peak shift can be attributed to the influence of magnetic field on the Young's modulus, i.e. the delta-E effect [38-40]. Comparing Figure 2a and 2b, it is interesting to note that the V_{out} at H_{bias}=2.5 Oe is dramatically enhanced by twice than that at zero field.

In order to search the optimal DC bias magnetic field, the DC field was scanned in the range of 0-15 Oe under a resonance frequency of 60.101 kHz. Figure 3 shows the V_{out}-H_{dc} curve and its differential. As illustrated, the V_{out} reaches the maximum around 2.5 Oe. Therefore, 2.5 Oe is the optimal DC bias field for AC magnetic field measurement (H_{bias}^{AC}). The differential (dV_{out}/dH_{dc}) curve of V_{out}-H_{dc} relationship represents the variation rate of the V_{out} with the external DC magnetic field. The magnetic field at the maximum of the differential curve $(dV_{out}/dH_{dc})_{max}$ is the optimal bias field for the DC magnetic field measurement (H_{bias}^{DC}), where the output voltage is most sensitive to the variation of DC magnetic field. From Figure 3, it can be seen that $(dV_{out}/dH_{dc})_{max}$ occurs at 0.5 Oe (i.e. H_{bias}^{DC}=0.5 Oe).

Preprints (www.preprints.org) | NOT PEER-REVIEWED | Posted: 28 December 2022 doi:10.20944/preprints202212.0528.v1

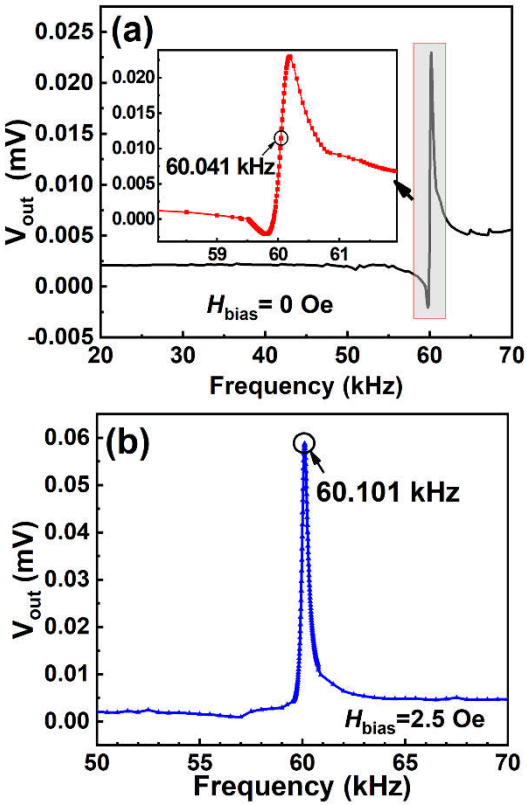

Figure 2. The frequency dependence of the V_{out} of the ME sensor without DC bias field H_{bia}=0 Oe (**a**) and with H_{bias}= 2.5 Oe (**b**). The inset of Figure 2a is a magnified view of the vicinity of the resonance peak.

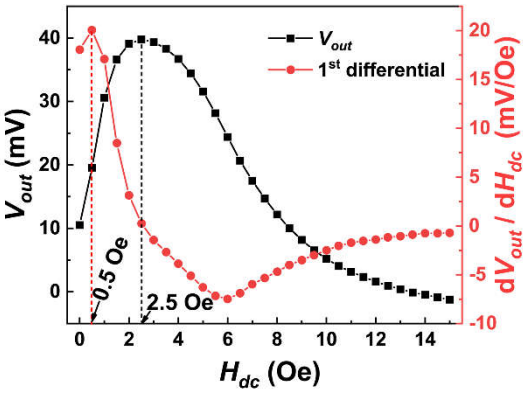

Figure 3. The V_{out}-H_{dc} curve and its differential curve at f_{res} of 60.101 kHz.

The resonant frequency of 60.101 kHz and the bias field of 2.5 Oe are adopted as the working point for AC field resolution measurement. The V_{out}-time steps at various input AC fields are shown in Figure 4. The absolute height of V_{out}-time step refers to the output voltage V_{out} at a certain AC voltage input to the long-straight solenoid, which can be converted to the input AC magnetic field intensity H_{in} after caliberation. Thus the relative height of the neighboring V_{out}-time steps can be converted as the difference of AC field ΔH_{in}. In other word, if the H_{in} is continuously reduced till the step height is indistinguishable, the corresponding ΔH_{in} is the resolution limit of the AC magnetic field H_{rsl}^{AC}. As illustrated in Figure 4, an excellent H_{rsl}^{AC} of 0.2 nT was obtained at resonance frequency of 60.101 kHz.

Preprints (www.preprints.org) | NOT PEER-REVIEWED | Posted: 28 December 2022 doi:10.20944/preprints202212.0528.v1

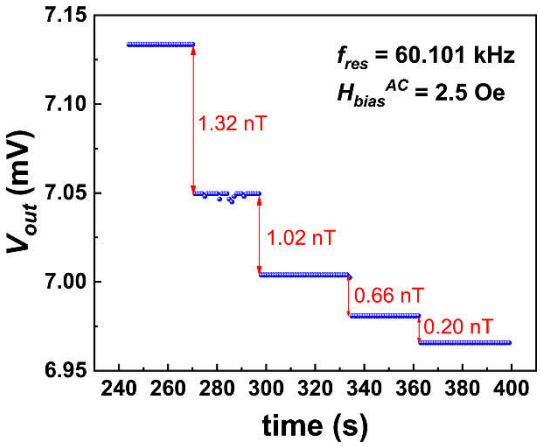

Figure 4. AC magnetic field resolution at f_{res} of 60.101 kHz and H_{bias}^{AC} of 2.5 Oe.

Similarly, the DC field resolution H_{rsl}^{DC} can be obtained under the working point with f_{res}= 60.101 kHz and H_{bias}^{DC}=0.5 Oe, as shown in Figure 5. The red dotted line represents the output voltage V_{out} of the ME sensor operating at the above working point without the DC perturbation magnetic field $[(V_{out})_0]$, which can be used as a reference voltage without input DC magnetic field. The optimal DC bias field H_{bias}^{DC}=0.5 Oe is supplied by the Helmholtz coils. The DC field to be measured H_{tbm}^{DC}, which has an opposite direction with the H_{bias}^{DC}, is generated by the small solenoid, supplied by Keithley 2400 source meter. If a H_{tbm}^{DC} (for example 5.0 nT) exerts on the ME sensor, the V_{out}-time step will decrease from 5.97 mV to 2.91 mV (Figure 5). If the DC input field H_{tbm}^{DC} is removed, the V_{out} is recovered to its original value. Gradually reducing the H_{tbm}^{DC} value till the V_{out}-time step cannot be distinguished from the base line, the DC magnetic field resolution H_{rsl}^{DC} will be obtained. As illustrated in Figure 5, a very low H_{rsl}^{DC} of 0.34 nT was achieved in this study. The $[(V_{out})_0]$ is close to the V_{out} under AC magnetic field measurement conditions, which indicates that the addition of a signal-free solenoid will cause a change in the corresponding magnetic field near the sensor, thereby changing the output signal; Moreover, the difference between the steps in Figure 5 and Figure 4 corresponds to different values, because different solenoids have different ability to convert magnetic fields, and the steps in measuring AC magnetic field are more stable than those in measuring DC magnetic field, indicating that the sensor has better ability to resist noise.

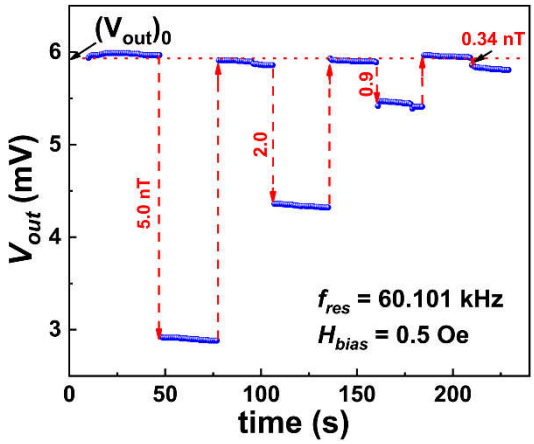

Figure 5. DC magnetic field resolution H_{rsl}^{DC} at f_{res}=60.101 kHz and H_{bias}^{DC}=0.5 Oe.

Preprints (www.preprints.org) | NOT PEER-REVIEWED | Posted: 28 December 2022 doi:10.20944/preprints202212.0528.v1

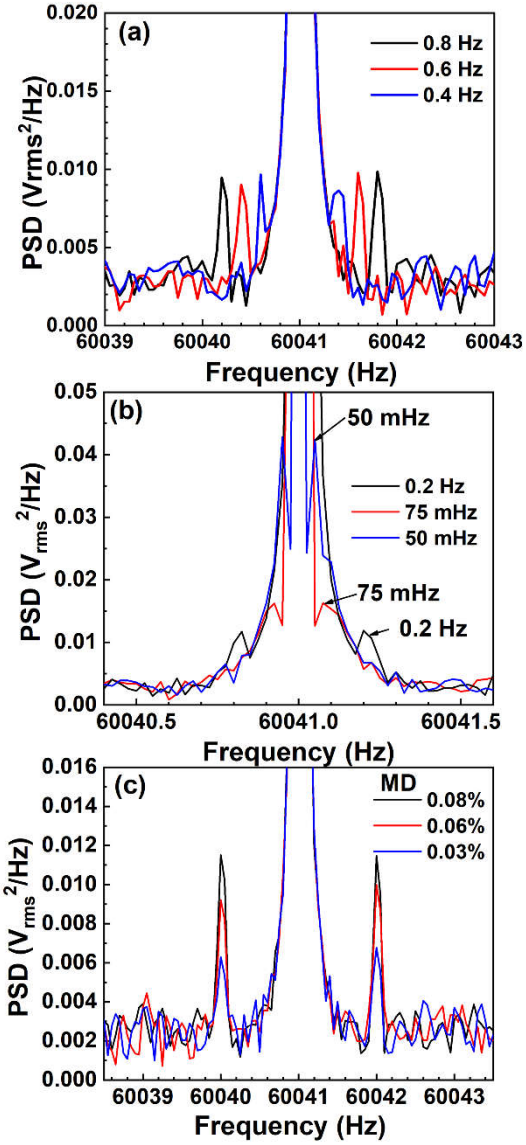

Figure 6. The modulation peaks at MD = 0.05% at various modulation frequencies (**a**) and (**b**), and at different MDs with a modulation frequency of 1 Hz (**c**).

As discussed above, the optimal AC field sensitivity of the ME sensors occurs at working point with f_{res}= 60.041 kHz@H_{bias}^{AC} = 2.5 Oe. In order to measure the ultralow frequency field, a FUCT method was proposed. In this method, another magnetic field H_{tbm}^{AC} with a low frequency f_{tbm}, as a field to be measured, was mixed with the AC exciting field H_{ac} at resonance frequency, leading to two shoulder peaks located at the left and right sides of the main peak with a frequency shift of $\pm f_{tbm}$. The intensity of the H_{tbm}^{AC} and the frequency f_{tbm} can be tuned by varying the modulation depth (MD=H_{tbm}^{AC}/H_{ac}) and frequency of the signal source [30]. Figure 6a and 6b show the influence of the modulation frequency on location of the shoulder peaks at a MD of 0.5%. As illustrated in Figure 6a, although the operating frequency is higher than 60 kHz, the modulated shoulder peaks at frequency differences of 0.4, 0.6, 0.8 Hz are clearly distinguishable. If further decreasing the modulation frequency, a modulation signal with an ultralow frequency of 50 mHz also can be distinguished from the background signal (Figure 6b). This indicates that the measurement instrument can detect the ultralow frequency magnetic field with frequency as low as 50 mHz. If fixing a modulation frequency (1 Hz for instance), the peak voltage of the shoulder peaks is proportional to the MD (i.e. the H_{tbm}^{AC}). The AC field resolution H_{rsl}^{AC} can be approaching by reducing the MD at the modulation frequency till the shoulder peaks cannot be distinguished from the background signal. Using this method,

Preprints (www.preprints.org) | NOT PEER-REVIEWED | Posted: 28 December 2022 doi:10.20944/preprints202212.0528.v1

the AC field resolutions H_{rsl}^{AC} in the frequency range from 80 Hz to 50 mHz were measured and summarized in Figure 7. As illustrated, the H_{rsl}^{AC} is dramatically deteriorated with the decreases of frequency. The H_{rsl}^{AC} rapidly increases from 0.45 nT@80 Hz to 51 nT@50 mHz. Nevertheless, for the frequency over 8 Hz, the H_{rsl}^{AC} of the ME sensor is better than 1 nT, which is an excellent achievement [5, 37, 41, 42].

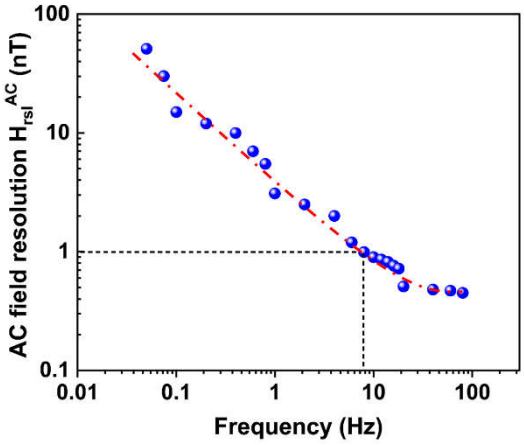

Figure 7. The AC magnetic field resolution at ultralow frequencies (the dash-dot line is guided for eyes).

4. Conclusions

A FeCoSiB Metglas/PZT-5B magnetoelectric coupling sensor with dimension of 25×2×0.5 mm^3 and resonance frequency of 60.101 kHz was fabricated for weak magnetic field measurement. It is interesting that excellent AC and DC magnetic field resolutions as low as 0.2 and 0.34 nT, respectively, were obtained. The frequency upconversion technique is an effective way to sensitively measure ultralow frequency AC magnetic field resolution. It is revealed that the AC field resolution is rapidly deteriorated with the decrease of frequency due to the far deviation from the resonance frequency. Nevertheless, an excellent AC field resolution is achieved, and the frequency of magnetic field resolution better than 1 nT consistently persists up to 8 Hz.

Author Contributions: K. Sun，**Z. Jiang**，**C. Wang**，and **D. Han**: Investigation, Writing - original draft, Data curation. **Z. Yao, W. Zong** and **Z. Jin**: Investigation, Data curation. **S. Li**: Supervision, Conceptualization, Methodology, Project administration.

Fundings: This work was financially supported by National Natural Science Foundation of China with grant No. 51871127 and 11674187.

Conflicts of Interests: The authors declare that they have no known competing financial interests or personal relationships that could have appeared to influence the work reported in this paper.

References

[1] Clausi, D.; Gradin, H.; Braun, S.; Peirs, J.; Stemme, G.; Reynaerts D.; van der Wijingaart, W. Robust actuation of silicon MEMS using SMA wires integrated at wafer-level by nickel electroplating. *Sensors and Actuators A: Physical* **2013**, *189*, 108-116. https://dx.doi.org/10.1016/j.sna.2012.08.036.

[2] Lee, H.-S.; Cho, C.; Chang, S.-P. Effect of SmFe and TbFe film thickness on magnetostriction for MEMS devices. *Journal of Materials Science* **2006**, *42*, 384-388. https://dx.doi.org/10.1007/s10853-006-1183-4.

[3] Liang, X.; Dong, C.; Chen, H.; Wang, J.; Wei, Y.; Zaeimbashi, M.; He, Y.; Matyushov, A.; Sun, C.; Sun, N. A review of thin-film magnetoelastic materials for magnetoelectric applications. *Sensors* **2020**, *20*, 1532-1558. https://dx.doi.org/10.3390/s20051532.

Preprints (www.preprints.org) | NOT PEER-REVIEWED | Posted: 28 December 2022 doi:10.20944/preprints202212.0528.v1

[4] Marauska, S.; Jahns, R.; Greve, H.; Quandt, E.; Knöchel, R.; and Wagner, B. MEMS magnetic field sensor based on magnetoelectric composites. *Journal of Micromechanics and Microengineering* **2012**, *22*, 065024-065029. https://dx.doi.org/10.1088/0960-1317/22/6/065024.

[5] Marauska, S.; Jahns, R.; Kirchhof, C.; Claus, M.; Quandt, E.; Knöchel, R.; Wagner, B. Highly sensitive wafer-level packaged MEMS magnetic field sensor based on magnetoelectric composites. *Sensors and Actuators A: Physical* **2013**, *189*, 321-327. https://dx.doi.org/10.1016/j.sna.2012.10.015.

[6] Preisner, T.; Klinkenbusch, L.; Bolzmacher, C.; Gerber, A.; Bauer, K.; Quandt, E.; Mathis, W. Numerical modeling of a MEMS actuator considering several magnetic force calculation methods. *COMPEL - The international journal for computation and mathematics in electrical and electronic engineering*. **2011**, *30*, 1176-1188. https://dx.doi.org/10.1108/03321641111133118.

[7] Li, J.; Ma, G.; Zhang, S.; Wang, C.; Jin, Z.; Zong, W.; Zhao, G.; Wang, X.; Xu, J.; Cao, D.; and Li, S. AC/DC dual-mode magnetoelectric sensor with high magnetic field resolution and broad operating bandwidth. *AIP Advances* **2021**, *11*, 045015-045021. https://dx.doi.org/10.1063/5.0048167.

[8] O'Reilly, J.M.; Stamenov, P. SQUID-detected FMR: Resonance in single crystalline and polycrystalline yttrium iron garnet. *Review of Scientific Instruments* **2018**, *89*, 044701-044711. https://dx.doi.org/10.1063/1.5009731.

[9] Tavassolizadeh, A.; Rott, K.; Meier, T.; Quandt, E.; Holscher, H.; Reiss, G.; Meyners, D. Tunnel magnetoresistance sensors with magnetostrictive electrodes: strain sensors. *Sensors* **2016**, *16*, 1902-1912. https://dx.doi.org/10.3390/s16111902.

[10] Chu, Z.; PourhosseiniAsl, M.; and Dong, S. Review of multi-layered magnetoelectric composite materials and devices applications. *Journal of Physics D: Applied Physics* **2018**, *51*, 243001-243036. https://dx.doi.org/10.1088/1361-6463/aac29b.

[11] Chu, Z.; Shi, H.; PourhosseiniAsl, M.J.; Wu, J.; Shi, W.; Gao, X.; Yuan, X.; Dong, S. A magnetoelectric flux gate: new approach for weak DC magnetic field detection. *Scientific Reports* **2017**, *7*, 8592-8599. https://dx.doi.org/10.1038/s41598-017-09420-w.

[12] PourhosseiniAsl, M.J.; Chu, Z.; Gao, X.; Dong, S. A hexagonal-framed magnetoelectric composite for magnetic vector measurement. *Applied Physics Letters* **2018**, *113*, 092902- 092906. https://dx.doi.org/10.1063/1.5022094.

[13] Schmid, U.; Giouroudi, I.; Alnassar, M.; Kosel, J.; Sánchez de Rojas Aldavero, J.L.; Leester-Schaedel, M. Fabrication and properties of $SmFe_2$-PZT magnetoelectric thin films. *Proceedings of SPIE - The International Society for Optical Engineering* **2013**, *8763*. https://repository.kaust.edu.sa/handle/10754/555694.

[14] Zhai, J.; Dong, S.; Xing, Z.; Li, J.; and Viehland, D. Geomagnetic sensor based on giant magnetoelectric effect. *Applied Physics Letters* **2007**, *91*, 123513-123516. https://dx.doi.org/10.1063/1.2789391.

[15] Chu, Z.; Gao, X.; Shi, W.; MohammdJavad, P.; Dong, S. A square-framed ME composite with inherent multiple resonant peaks for broadband magnetoelectric response. *Science Bulletin* **2017**, *62*, 1177-1180. https://dx.doi.org/10.1016/j.scib.2017.08.017.

[16] Chu, Z.; Annapureddy, V.; PourhosseiniAsl, M.; Palneedi, H.; Ryu, J.; Dong, S. Dual-stimulus magnetoelectric energy harvesting. *MRS Bulletin* **2018**, *43*, 199-205. https://dx.doi.org/10.1557/mrs.2018.31.

[17] Röbisch, V.; Salzer, S.; Urs, N.O.; Reermann, J.; Yarar, E.; Piorra, A.; Kirchhof, C.; Lage, E.; Höft, M.; Schmidt, G.U.; Knöchel, R.; McCord, J.; Quandt, E.; Meyners, D. Pushing the detection limit of thin film magnetoelectric heterostructures. *Journal of Materials Research* **2017**, *32*, 1009-1019. https://doi.org/10.1557/jmr.2017.58.

[18] Hayes, P.; Jovicevic Klug, M.; Toxvaerd, S.; Durdaut, P.; Schell, V.; Teplyuk, A.; Burdin, D.; Winkler, A.; Weser, R.; Fetisov, Y.; Hoft, M.; Knochel, R.; McCord, J.; and Quandt, E. Converse magnetoelectric composite resonator for sensing small magnetic fields. *Scientific Reports* **2019**, *9*, 16355-16364. https://dx.doi.org/10.1038/s41598-019-52657-w.

[19] Hoffmann, J.; Hansen, C.; Maetzler, W.; Schmidt, G. A concept for 6D motion mensing with magnetoelectric mensors. *Current Directions in Biomedical Engineering* **2022**, *8*, 451-454. http://doi.org/10.1515/cdbme-2022-1115.

[20] Elzenheimer, E.; Bald, C.; Engelhardt, E.; Hoffmann, J.; Hayes, P.; Arbustini, J.; Bahr, A.; Quandt, E.; Hoft, M.; Schmidt, G. Quantitative evaluation for magnetoelectric sensor systems in biomagnetic diagnostics. *Sensors* **2022**, *22*, 5675-5691. http://doi.org/10.3390/s22031018.

[21] Baek, G.; Yang, S.C. Effect of the two-dimensional magnetostrictive fillers of $CoFe_2O_4$-intercalated graphene oxide sheets in 3-2 type poly(vinylidene fluoride)-based magnetoelectric films. *Polymers* **2021**, *13*, 1782-1795. https://dx.doi.org/10.3390/polym13111782.

[22] Castro, N.; Reis, S.; Silva, M.P.; Correia, V.; Lanceros-Mendez, S.; Martins, P. Development of a contactless DC current sensor with high linearity and sensitivity based on the magnetoelectric effect. *Smart Materials and Structures* **2018**, *27*, 065012-065018. https://dx.doi.org/10.1088/1361-665X/aab969.

[23] Lu, C.; Li, P.; Wen, Y.; Yang, A.; He, W.; Zhang, J. Enhancement of resonant magnetoelectric effect in magnetostrictive/piezoelectric heterostructure by end bonding. *Applied Physics Letters* **2013**, *102*, 132410-132413. https://dx.doi.org/10.1063/1.4799967.

[24] Pandya, S.; Wilbur, J.D.; Bhatia, B.; Damodaran, A.R.; Monachon, C.; Dasgupta, A.; King, W.P.; Dames, C.; and Martin, L.W. Direct measurement of pyroelectric and electrocaloric effects in thin films. *Physical Review Applied* **2017**, *7*, 034025-134037. https://dx.doi.org/10.1103/PhysRevApplied.7.034025.

[25] Li, M.; Wang, Z.; Wang, Y.; Li, J.; Viehland, D. Giant magnetoelectric effect in self-biased laminates under zero magnetic field. *Applied Physics Letters* **2013**, *102*, 082404-082406. https://dx.doi.org/10.1063/1.4794056.

[26] Bichurin, M.I.; Petrov, V.M.; and Srinivasan, G. Theory of low-frequency magnetoelectric coupling in magnetostrictive-piezoelectric bilayers. *Physical Review B* **2003**, *68*, 054402-054414. https://dx.doi.org/10.1103/PhysRevB.68.054402.

[27] Röbisch, V.; Piorra, A.; Lima de Miranda, R.; Quandt, E.; Meyners, D. Frequency-tunable nickel-titanium substrates for magnetoelectric sensors. *AIP Advances* **2018**, *8*, 125320-125326. https://dx.doi.org/10.1063/1.5066076.

Preprints (www.preprints.org) | NOT PEER-REVIEWED | Posted: 28 December 2022 doi:10.20944/preprints202212.0528.v1

[28] Su, J.; Niekiel, F.; Fichtner, S.; Kirchhof, C.; Meyners, D.; Quandt, E.; Wagner, B.; and Lofink, F. Frequency tunable resonant magnetoelectric sensors for the detection of weak magnetic field. *Journal of Micromechanics and Microengineering* **2020**, *30*, 075009-075006. https://dx.doi.org/10.1088/1361-6439/ab8dd0.

[29] Röbisch, V.; Yarar, E.; Urs, N.O.; Teliban, I.; Knöchel, R.; McCord, J.; Quandt, E.; Meyners, D. Exchange biased magnetoelectric composites for magnetic field sensor application by frequency conversion. *Journal of Applied Physics* **2015**, *117*, 17B513-17B516. https://dx.doi.org/10.1063/1.4913814.

[30] Li, J.; Sun, K.; Jin, Z.; Li, Y.; Zhou, A.; Huang, Y.; Yang, S.; Wang, C.; Xu, J.; Zhao, G.; Wang, X.; Cao, D.; Zong, W.; Li, S. A working-point perturbation method for the magnetoelectric sensor to measure DC to ultralow-frequency-AC weak magnetic fields simultaneously. *AIP Advances* **2021**, *11*, 065213-065219. https://dx.doi.org/10.1063/5.0047490.

[31] Jiao, J.; Zhang, H.; Liu, Y.; Fang, C.; Lin, D.; Zhao, X.; Luo, H. Influence of metglas layer on nonlinear magnetoelectric effect for magnetic field detection by frequency modulation. *Journal of Applied Physics* **2015**, *117*, 024104-024109. https://dx.doi.org/10.1063/1.4905622.

[32] Pan, L.; Pan, M.; Hu, J.; Hu, Y.; Che, Y.; Yu, Y.; Wang, N.; Qiu, W.; Li, P.; Peng, J.; Jiang, J. Novel magnetic field modulation concept using multiferroic heterostructure for magnetoresistive sensors. *Sensors* **2020**, *20*, 1440-1442. https://dx.doi.org/10.3390/s20051440.

[33] Ren, S.; Xue, D.; Ji, Y.; Liu, X.; Yang, S.; Ren, X. Low-field-triggered large magnetostriction in iron-palladium strain glass alloys. *Physical Review Letters* **2017**, *119*, 125701-125706. https://dx.doi.org/10.1103/PhysRevLett.119.125701.

[34] Lu, Y.; Cheng, Z.; Chen, J.; Li, W.; and Zhang, S. High sensitivity face shear magneto-electric composite array for weak magnetic field sensing. *Journal of Applied Physics* **2020**, *128*, 064102-064109. https://dx.doi.org/10.1063/5.0011931.

[35] Chu, Z.; Dong, C.; Tu, C.; Liang, X.; Chen, H.; Sun, C.; Yu, Z.; Dong, S.; Sun, N.-X. A low-power and high-sensitivity magnetic field sensor based on converse magnetoelectric effect. *Applied Physics Letters* **2019**, *115*, 162901-162905. https://dx.doi.org/10.1063/1.5122774.

[36] Shi, J.; Wu, M.; Hu, W.; Lu, C.; Mu, X.; Zhu, J. A study of high piezomagnetic (Fe-Ga/Fe-Ni) multilayers for magnetoelectric device. *Journal of Alloys and Compounds* **2019**, *806*, 1465-1468. https://dx.doi.org/10.1016/j.jallcom.2019.07.265.

[37] Hayes, P.; Schell, V.; Salzer, S.; Burdin, D.; Yarar, E.; Piorra, A.; Knöchel, R.; Fetisov, Y.K.; Quandt, E. Electrically modulated magnetoelectric AlN/FeCoSiB film composites for DC magnetic field sensing. *Journal of Physics D: Applied Physics* **2018**, *51*, 116486-116490. https://dx.doi.org/10.1088/1361-6463/aad456.

[38] Zabel, S.; Reermann, J.; Fichtner, S.; Kirchhof, C.; Quandt, E.; Wagner, B.; Schmidt, G.; Faupel, F. Multimode delta-E effect magnetic field sensors with adapted electrodes. *Applied Physics Letters* **2016**, *108*, 222401-222404. https://dx.doi.org/10.1063/1.4952735.

[39] Spetzler, B.; Bald, C.; Durdaut, P.; Reermann, J.; Kirchhof, C.; Teplyuk, A.; Meyners, D.; Quandt, E.; Hoft, M.; Schmidt, G.; Faupel, F. Exchange biased delta-E effect enables the detection of low frequency pT magnetic fields with simultaneous localization. *Scientific Reports* **2021**, *11*, 5269-5282. http://doi.org/10.1038/s41598-021-84415-2.

[40] Bald, C.; Schmidt, G. Processing chain for localization of magnetoelectric sensors in real time. *Sensors* **2021**, *21*, 5675-5691. http://doi.org/10.3390/s21165675.

[41] Das, J.; Gao, J.; Xing, Z.; Li, J.F.; Viehland, D. Enhancement in the field sensitivity of magnetoelectric laminate heterostructures. *Applied Physics Letters* **2009**, *95*, 092501-092503. https://dx.doi.org/10.1063/1.3222914.

[42] Lu, C.; Li, P.; Wen, Y.; Yang, A.; Yang, C.; Wang, D.; He, W.; Zhang, J. Magnetoelectric composite metglas/PZT-based current sensor. *IEEE Transactions on Magnetics* **2014**, *50*, 1-4. https://dx.doi.org/10.1109/tmag.2014.2326193.